PCCP

PAPER

View Article Online
View Journal | View Issue

Excitation wavelength dependence of the charge separation pathways in tetraporphyrin-naphthalene diimide pentads†

Cite this: *Phys. Chem. Chem. Phys.*, 2014, **16**, 5188

Diego Villamaina,[a] Melissa M. A. Kelson,[b] Sheshanath V. Bhosale*[b] and Eric Vauthey*[a]

Received 19th November 2013,
Accepted 21st January 2014

DOI: 10.1039/c3cp54871f

www.rsc.org/pccp

The excited-state dynamics of two multichromophoric arrays composed of a naphthalene diimide centre and four zinc or free-base porphyrins substituted on the naphthalene core *via* aniline bridges has been investigated using a combination of stationary and ultrafast spectroscopy. These pentads act as efficient antennae as they absorb over the whole visible region, with a band around 700 nm, associated with a transition to the S_1 state delocalised over the whole arrays, and bands at higher energy due to transitions centred on the porphyrins. In non-polar solvents, population of these porphyrin states is followed by sub-picosecond internal conversion to the S_1 state. The existence of a charge-separated state located above the S_1 state could enhance this process. The decay of the S_1 state is dominated by non-radiative deactivation on the 100 ps timescale, most probably favoured by the small S_1–S_0 energy gap and the very high density of vibrational states of these very large chromophores. In polar solvents, the charge-separated state lies just below the S_1 state. It can be populated within a few picoseconds by a thermally activated hole transfer from the S_1 state as well as *via* sub-picosecond non-equilibrium electron transfer from vibrationally hot porphyrin excited states. Because of the small energy gap between the charge-separated state and the ground state, charge recombination is almost barrierless and occurs within a few picoseconds. Despite their very different driving forces, charge separation and recombination occur on similar timescales. This is explained by the electronic coupling that differs considerably for both processes.

Introduction

Over the past years, our understanding of the mechanisms of electronic energy migration and charge separation in the photosynthetic apparatus of plants and bacteria has made tremendous progress.[1–7] In parallel, strong efforts have been invested in the design and synthesis of artificial analogues of the light harvesting complexes and reaction centres.[8–14] The high efficiency of natural antennae complexes lies in their ability to collect sunlight across all of the visible region due to the presence of various pigments embedded in the proteinic environment. The mutual spatial arrangement of these pigments is such that it ensures efficient electronic energy transport and prevents aggregation that would lead to a rapid conversion of the electronic energy into heat. To mimic these systems, a large variety of covalently linked and self-assembled arrays of chromophores have been synthesised and investigated.[15–27] Porphyrins, especially zinc and free-base porphyrins, are among the most used chromophoric units. However, despite their structural resemblance to the chlorophylls, their extinction coefficient in the visible region is considerably smaller, and because of their higher symmetry most of their cross section for absorption is concentrated in the intense Soret or B band located around 420 nm. Therefore, porphyrins should be combined with other chromophores to realise more practical antennae. Core-substituted naphthalene diimides (c-NDIs) have been shown to be extremely versatile chromophoric building blocks for the construction of sophisticated molecular architectures with various applications such as *e.g.* sensing, photovoltaics and charge transport.[28–34] Whereas core-unsubstituted NDIs do not absorb in the visible region and have a small fluorescence quantum yield,[35–37] the presence of electron-donating substituents on the naphthalene core results in a new electronic absorption band located at lower energy due to a charge-transfer type transition.[38] This new band can be continuously shifted throughout the

[a] *Dpt. of Physical Chemistry, University of Geneva, 30 quai Ernest-Ansermet, CH-1211 Geneva, 4, Switzerland. E-mail: eric.vauthey@unige.ch*
[b] *School of Applied Sciences, RMIT University, GPO Box 2476, Melbourne, Victoria 3001, Australia. E-mail: sheshanath.bhosale@rmit.edu.au*

† Electronic supplementary information (ESI) available: Synthesis of the arrays, fluorescence up-conversion data for array **1**, decay associated fluorescence spectra, transient absorption spectra measured with array **2**. Calculation of the excitation energy hopping rate constants. See DOI: 10.1039/c3cp54871f

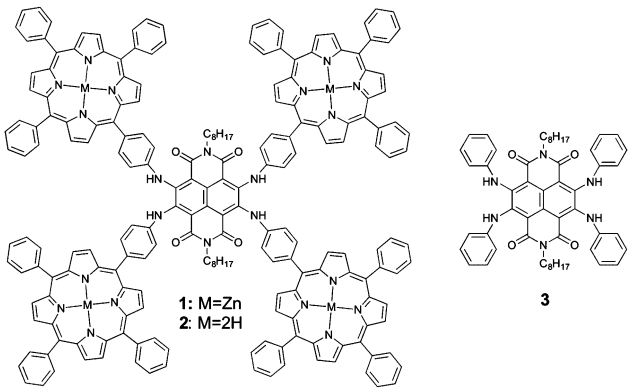

Scheme 1

whole visible region depending on the number and the electron-donating strength of the substituents. The smallest S_1–S_0 energy gap achieved so far has been realised with either four *N*-alkylamino or two ethynyl-*N*,*N*-dihexylaniline substituents and amounts to 1.79 eV (690 nm).[39,40] Most c-NDIs have a fluorescence lifetime of several nanoseconds and a fluorescence quantum yield of the order of 0.5. Additionally, varying the core substituents allows for a continuous tuning of the redox properties of c-NDIs, making them extremely powerful building blocks of photoactive charge-transfer cascades.

We report here on our investigation of the excited-state properties of two new multichromophoric arrays (Scheme 1) consisting of a central c-NDI unit substituted at the core by four zinc (ZnP, array **1**) or free-base tetraphenylporphines (FbP, array **2**). Our motivation was to realise molecular arrays acting at the same time as antennae, absorbing in most of the visible region due to the combination of four porphyrins and one c-NDI, and undergoing subsequent charge separation (CS). Contrary to the natural complexes and to most of their artificial analogues, the chromophoric units of **1** and **2** are active in both the light collection and the CS steps. The covalent binding of an electron donor to the core of a NDI has been shown to lead to CS faster by three orders of magnitude than the more conventional binding to the imide N atom.[41] Despite this, the number of donor–acceptor (D–A) systems based on core substitution of NDI is still relatively limited.[42,43] We have recently described D–A dyads and D–A–D triads, based on porphyrins and c-NDIs.[44,45] In the first case, the porphyrin, either ZnP or FbP, was linked through a rigid diaza bridge to the core of a c-NDI.[44] Such rigid bridging resulted in a strong coupling between the two chromophoric units, and as a consequence, the electronic excitation was delocalised over the whole molecule. This large coupling favoured ultrafast (1–3 ps) CS from the porphyrin to the c-NDI in medium polarity solvents, despite a modest driving force ($-\Delta G_{CS} \sim 0.1$ eV) and rapid (10–20 ps) charge recombination (CR). In the triads, the porphyrins were directly connected to the core of the NDI through one of their phenyl substituents, giving significantly greater conformational flexibility and hence reducing the coupling.[45] As a result, the electronic excitation remained localised on one chromophoric unit. As the first absorption band of the tetraphenyl c-NDI strongly overlapped with the intense Soret band of the porphyrin, the c-NDI could not be selectively excited and made a small contribution to the overall absorption of the triads in the visible region. Photo-induced CS from the porphyrin to the c-NDI was found to be about 20 times faster with ZnP than with FbP, indicating that, contrary to the dyads, the controlling factor for CS was the driving force and not the electronic coupling.

The pentads investigated here differ from the above-mentioned triads, not only because of the larger number of porphyrin units, but mainly because of the nature of the central c-NDI that exhibits substantial absorbance in a spectral region where the porphyrins are mostly transparent. This is due to the presence of the four amino core substituents that results in a $S_1 \leftarrow S_0$ transition above 600 nm.[39] This also allows both the porphyrins and the c-NDI to be selectively photo-excited. We will show that the pentads exhibit significantly more complicated excited-state dynamics than the above dyads and triads, as it depends on whether a porphyrin or the c-NDI is initially excited, and that these arrays indeed combine some of the properties desired for an artificial antenna and reaction centre, namely very efficient energy collection and charge separation.

Experimental section

Samples

The solvents, toluene (Fisher analytical grade) and benzonitrile (Fluka puriss.), were used as received. The synthesis of the pentads **1** and **2** is described in detail in the ESI.† In brief, **1** and **2** were synthesised by the condensation of *N*,*N*′-bis(*n*-octyl)-2,3,6,7-tetrabromonaphthalene diimide **4** with 5-(4-aminophenyl)-10,15,20-triphenylporphyrin **5** under an argon atmosphere for 12 h in dry DMF at 135 °C, giving crystalline green-purple solid of **2** with 45% yield. **1** was obtained as a purple solid by metallation of **2** with $Zn(OAc)_2$ in $CHCl_3$/MeOH (20 : 1) at room temperature with 96% yield.

Spectroscopic measurements

Absorption spectra were measured on a Cary 50 spectrometer, whereas fluorescence emission and excitation spectra were recorded on a Cary Eclipse fluorometer. All emission spectra were corrected for the wavelength dependence sensitivity of the detector. The fluorescence quantum yields, Φ_f, were determined using oxazine 725 in ethanol as a reference ($\Phi_f = 0.14$).[46]

Nanosecond fluorescence dynamics was measured by time-correlated single photon counting (TCSPC) as described in ref. 47 and 48, using ~60 ps excitation pulses at 395 nm, generated at 10 MHz by a laser diode (Picoquant, LDH-P-C-400B). The full width at half maximum (fwhm) of the instrument response function (irf) was around 200 ps.

Faster fluorescence dynamics was monitored by fluorescence up-conversion (FU) as described elsewhere.[49,50] Excitation was performed at 420 nm with the frequency-doubled output of a Kerr-lens mode-locked Ti:Sapphire laser (Mai Tai, Spectra Physics). The pump intensity on the sample was of the order of 5 μJ cm^{-2} and the fwhm of the irf was *ca.* 200 fs. The sample solutions were located in a 0.4 mm rotating cell and had an

absorbance of about 0.1 at 420 nm. The reconstruction of the time-resolved fluorescence spectra (TRES) from the time profiles measured at several wavelengths was performed as described in ref. 51.

The electronic transient absorption (TA) measurements have been carried out with the setup described in ref. 52 and 53. Excitation was performed at 400 nm using the frequency-doubled output of a standard 1 kHz amplified Ti:Sapphire system (Spectra Physics) and at 525, 550 and 670 nm with the output of a home-built two-stage non-collinear parametric amplifier. The pump intensity on the sample was *ca.* 0.15 mJ cm^{-2} at 400 nm and 0.5 mJ cm^{-2} at the other wavelengths. The polarisation of the probe pulses was at the magic angle relative to that of the pump pulses. The fwhm of the irf was around 150 fs. The sample solutions were located in a 1 mm quartz cell and were continuously stirred by N_2 bubbling. Their absorbance at the excitation wavelength was around 0.1 for 400 nm pump pulses and 0.05 for 525, 550 and 670 nm excitation. The average number of excitations per porphyrin was estimated to be of the order of 0.01. The probability to have more than one excitation per pentad, calculated with the binomial distribution,[54,55] was at most 1%.

Computational methods

Given the size and complexity of the arrays, several conformations can be expected at room temperature. Gas phase geometry optimisation was performed using the semi-empirical AM1 method with several possible conformations as initial geometries. The two most stable were then minimised at the density level of theory (DFT) using the B3LYP functional and the 6-31G* basis set. The structure of the most stable was then used to calculate the electronic transitions. The latter were computed in toluene with time-dependent DFT using the same functional and basis set, and with the polarised continuum formalism (PCM) for solvation. This approach has been shown to properly reproduce the electronic transition energies of zinc porphyrins.[56] All calculations were performed using Gaussian 09.[57] The structure described further in the text is probably not the only possible one. However, as the shape and relative energy of the frontier molecular orbitals were found to be qualitatively very similar in all the conformations investigated, these computational results can be reliably used to discuss the nature of the lowest electronic excited states of the arrays.

Results

Steady-state spectroscopy

The absorption spectra of the pentads **1** and **2** in toluene together with those of the constituents, namely ZnP, FbP and tetra(*n*-phenylamino)-NDI (**3**, Scheme 1), are shown in Fig. 1. Both arrays exhibit a very broad absorption spectrum covering most of the visible region. Their spectra are not the composite of those of the constituents, although contributions of the latter can be easily recognised. Indeed, the lowest energy band of **1** and **2** has a shape resembling that of **3**, but is centred at *ca.* 710 nm instead of 620 nm. This $\sim$2000 cm^{-1} red shift can be explained by the porphyrins, which enhance the donating

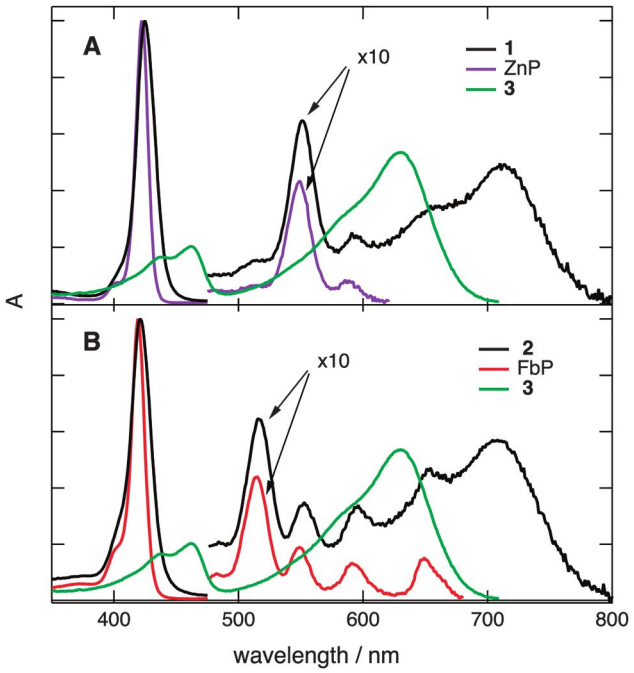

Fig. 1 Absorption spectra of **1** and **2** and of the individual constituents in toluene.

properties of the core substituents. One can thus infer that the excited-state associated with this first electronic transition is not entirely located on the c-NDI centre but involves the porphyrins as well. TD-DFT calculations predict that the first absorption band of both **1** and **2** in toluene is at 770 nm, and that it is associated with a one electron HOMO–LUMO transition. As depicted in Fig. 2 for **1** and Fig. S1, ESI† for **2**, the HOMO is delocalised over the whole array, whereas the LUMO is fully localised on the c-NDI centre. In this respect, the pentads can be considered as very large c-NDI dyes, and are, to our knowledge, the longest wavelength absorbing c-NDIs reported so far.[33,39,40] The close similarity of the $S_1 \leftarrow S_0$ bandshape of the pentads and **3** indicates that the $S_1 \leftarrow S_0$

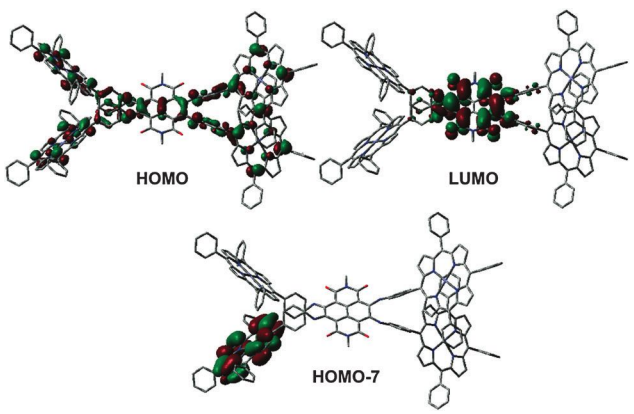

Fig. 2 Optimised geometry of **1** and most relevant molecular orbitals computed at the B3LYP/6-31G* level of theory (the H atoms are omitted for better visibility; the calculations have been done with methyl instead of octyl substituents on the imide N atoms).

excitation has little impact on the equilibrium geometry of the porphyrin substituents, but rather affects that of the NDI centre. This is not really surprising as the change of electronic density on each porphyrin upon $S_1 \leftarrow S_0$ excitation is rather modest compared to the change of electronic density on the NDI.

On the other hand, the Q bands are at the same position in the pentads spectra as in the ZnP and FbP spectra, indicating that the excited states associated with these transitions are mostly localised on the porphyrins. The quantum chemistry calculations point to the existence of MOs and virtual MOs centred on a single porphyrin unit (Fig. 2). Finally, the intense Soret or B band of the porphyrins is only slightly red shifted in the pentads (60 and 160 cm^{-1} for **1** and **2**, respectively) and is *ca.* 50% broader. These effects can be ascribed to the decrease of symmetry introduced by the linkage to the c-NDI. Additionally, the centre-to-centre distance between two adjacent porphyrins amounts to *ca.* 1.2 nm and, therefore, excitonic interaction could also contribute to the broadening of the B band as discussed in more detail below. Despite this, we will assume that the excited state populated upon excitation in the B band is mostly localised on one porphyrin unit. Hereafter, the state populated upon excitation in the lowest energy band will be called S_1 state, whereas those populated upon excitation in the Q and B bands will be named local Q and B states (L_Q and L_B), respectively.

In benzonitrile, the absorption spectra of **1** and **2** are essentially the same as in toluene, apart from minor (<150 cm^{-1}) shifts of the bands. The fluorescence spectra of the arrays are very similar and consist of a band with a shape close to the mirror image of the $S_1 \leftarrow S_0$ absorption band and with a maximum at *ca.* 770 nm (Fig. 3). They resemble the fluorescence spectrum of c-NDI **3** but are red-shifted by the same amount, *i.e.* $\sim$2000 cm^{-1}, as the absorption band. Very weak spectral features that coincide with the emission spectra of ZnP and FbP can be observed on the high energy side of the fluorescence band of the arrays. As it will be shown below, these features can be ascribed to the $L_Q \rightarrow S_0$ fluorescence.

The $S_1 \rightarrow S_0$ fluorescence excitation spectra of both pentads are essentially the same as their absorption spectra (Fig. S2, ESI†), pointing to very efficient internal conversion from the L_B and L_Q states to the S_1 states. These latter processes could also be viewed as a redistribution of the excitation energy from one porphyrin unit over the whole array. The fluorescence quantum yield of **3** was not determined but can be expected to be very close to the Φ_f value of 0.13 reported for a similar c-NDI with hexyl instead of phenyl substituents.[39] The fluorescence quantum yields of the pentads in toluene are substantially smaller, and amount to 0.013 and 9×10^{-3} for **1** and **2**, respectively. In the polar benzonitrile, the arrays are almost non-fluorescent with Φ_f values of 2×10^{-3} for **1** and 5×10^{-4} for **2**.

Time-resolved fluorescence

The fluorescence decay of the c-NDI **3** in toluene measured by TCSPC is exponential with a 3.9 ns lifetime. On the other hand, the fluorescence dynamics of the pentads in toluene was too fast to be properly resolved by TCSPC and was thus measured by FU. The FU time profiles in toluene are strongly wavelength dependent (Fig. 4A and Fig. S3, ESI†). Below 720 nm, the profiles exhibit a biphasic decay with a very fast component, whose relative amplitude decreases with increasing wavelength. Above 720 nm, the FU intensity shows a 1–2 ps rise and a decay on the 100 ps timescale. All time profiles could be analysed

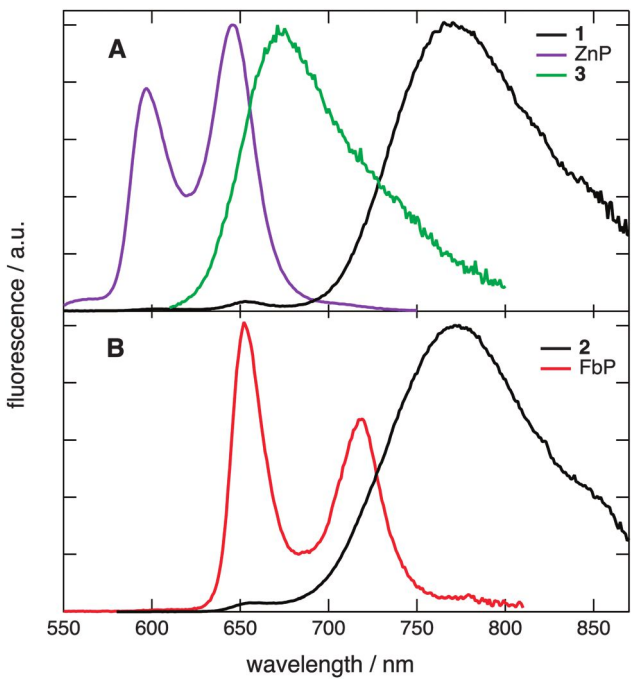

Fig. 3 Fluorescence spectra of **1** and **2** and of the individual constituents in toluene.

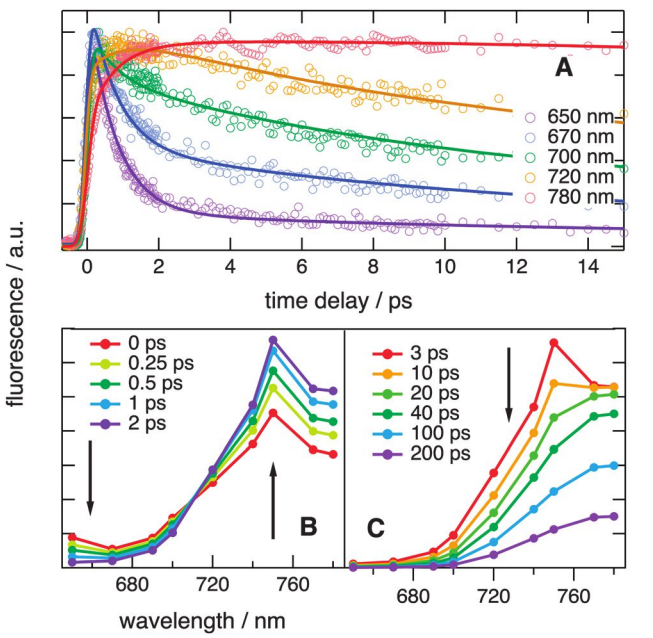

Fig. 4 (A) Time profiles of the fluorescence intensity measured at several wavelengths upon $L_B \leftarrow S_0$ excitation of **2** in toluene and the best fit obtained from a global multiexponential analysis (solid lines); (B and C) reconstructed time-resolved emission spectra.

Table 1 Time constants of $L_Q \rightarrow S_1$ internal conversion, vibrational cooling and S_1 state decay obtained from a global analysis of the fluorescence up-conversion data (limit of error: ±5%)

Array	Solvent	τ_{IC}/ps	τ_{VC}/ps	τ_{S1}/ps
1	Toluene	0.8	6.6	93
1	Benzonitrile	0.5		4.6
2	Toluene	0.8	11	145
2	Benzonitrile	0.6		12

globally with the sum of three exponential functions with the time constants listed in Table 1 and the decay-associated spectra shown in Fig. S4 (ESI†).

The decay-associated spectra together with the time-resolved fluorescence spectra (TRES) reconstructed from the time profiles using the procedure described in ref. 51 (Fig. 4B and Fig. S3, ESI†) reveal that these wavelength-dependent dynamics correspond to a decay of the fluorescence intensity below 710 nm and to a parallel rise at longer wavelengths. As the emission below 710 nm coincides with the $L_Q \rightarrow S_0$ fluorescence, the shortest time constant can be interpreted as the internal conversion from the L_Q state, itself populated upon internal conversion from the L_B state, to the S_1 state. This $L_Q \rightarrow S_1$ internal conversion can be viewed as a spread of the electronic energy from one peripheral porphyrin over the whole array. The longest time constant corresponds to the decay of the emission intensity above 710 nm and can thus be interpreted as the lifetime of the S_1 state. Finally, the intermediate time constant is related to a red shift of the S_1 emission band. In fact, this feature most probably corresponds to a narrowing of the band due to vibrational cooling.[58] Indeed, upon 420 nm excitation and internal conversion to the S_1 state, more than 1.4 eV are converted into vibrational energy.

In benzonitrile, $L_Q \rightarrow S_1$ internal conversion is also observed with both pentads but is apparently faster (Table 1). The decay of the S_1 state is also more than ten times faster than in toluene, in agreement with the vanishingly small fluorescence quantum yields.

ZnP is known to exhibit measurable fluorescence from the B state around 430 nm with a 1.5 ps lifetime in toluene.[59,60] No steady-state $L_B \rightarrow S_0$ fluorescence could be detected with **1** and the FU time profiles measured in the 430–460 nm region were essentially the same as the irf, pointing to a L_B state lifetime well below 100 fs. Similar shortening of the L_B fluorescence lifetime has been observed upon substitution of ZnP.[45,61–63]

Transient absorption (TA), $L_B \leftarrow S_0$ excitation

TA spectra measured at several time delays after 400 nm excitation of the pentads in toluene are shown in Fig. 5A and B and Fig. S5, ESI.† The spectra exhibit two negative bands, a narrow one centred around 420 nm, that can be ascribed to the bleach of the $L_B \leftarrow S_0$ absorption, and a broad one above 600 nm corresponding to the bleach of the $S_1 \leftarrow S_0$ absorption. The positive feature between 450 and 600 nm resembles that observed with the ZnP and FbP alone and can thus be ascribed to the absorption of the locally excited porphyrins.[64] During the first 2 ps after excitation, the $L_B \leftarrow S_0$ bleach decreases whereas the

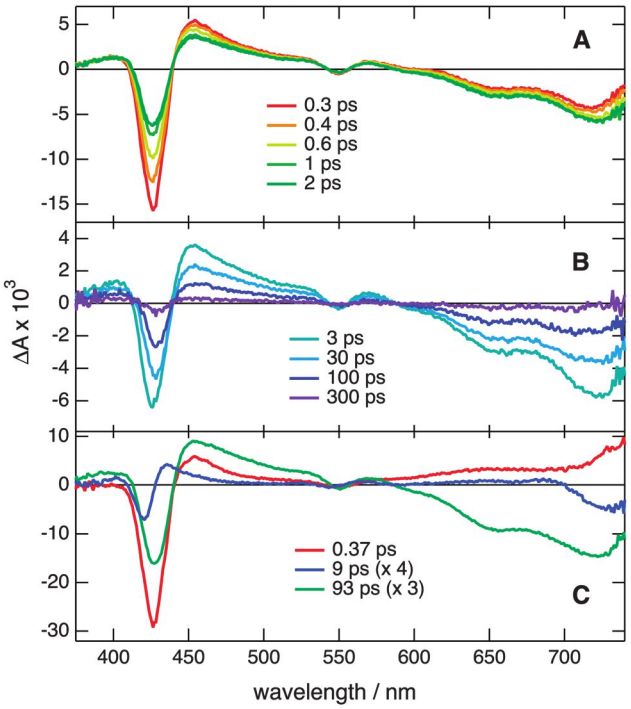

Fig. 5 (A and B) Transient absorption spectra measured at several time delays after $L_B \leftarrow S_0$ excitation of **1** in toluene and (C) decay-associated difference spectra obtained from a global multiexponential analysis.

$S_1 \leftarrow S_0$ bleach increases. This change can be ascribed to the $L_Q \rightarrow S_1$ internal conversion and confirms the above interpretation of the TRES. From *ca.* 2 ps onward, the overall shape of the TA spectra remains constant apart from a small red shift of the 420 nm negative band on an ~10 ps timescale (Fig. 5B), and the intensity decreases to zero within about 300 ps. The temporal evolution of the TA spectra was analysed globally and required the sum of at least three exponential functions to be properly reproduced. The resulting time constants are listed in Table 2, whereas the decay-associated difference spectra (DADS)[65] are depicted in Fig. 5C and Fig. S5, ESI.† The shortest time constant DADS reflects the ultrafast $L_Q \rightarrow S_1$ internal conversion. The longest time constant is very close to the S_1 fluorescence lifetime measured by FU and its DADS indicates that the S_1 state population decays directly to the ground state. Interestingly, although the $L_Q \rightarrow S_1$ internal conversion has taken place, the TA spectra still exhibit spectral features of porphyrins, namely

Table 2 Time constants obtained from the global analysis of the transient absorption spectra measured upon 400 and 670 nm excitation (limit of error: ±5%)

Array	Solvent	Excitation	τ_1/ps	τ_2/ps	τ_3/ps	τ_4/ps
1	Toluene	$L_B \leftarrow S_0$	0.4	9	93	
1	Toluene	$S_1 \leftarrow S_0$		11	93	
1	Benzonitrile	$L_B \leftarrow S_0$	0.3	3.2	4.6	22
1	Benzonitrile	$S_1 \leftarrow S_0$		3.2	4.6	20
2	Toluene	$L_B \leftarrow S_0$	0.6	16	145	
2	Toluene	$S_1 \leftarrow S_0$		28	140	
2	Benzonitrile	$L_B \leftarrow S_0$	0.5	13	33	
2	Benzonitrile	$S_1 \leftarrow S_0$		14	38	

the negative band around 420 nm. This is a further indication that the S_1 state of the array is not entirely centred on the c-NDI unit but is also delocalised on the porphyrin substituents.

The 10–20 ps DADS has a very similar shape for both arrays, with a dispersive-like feature around 410 nm. This time constant is similar to that found in the FU measurements and is ascribed to vibrational cooling. After $L_B \rightarrow L_Q$ and $L_Q \rightarrow S_1$ internal conversion, only about 1.7 eV of the 3.1 eV absorbed by the pentads remains as electronic energy. The difference is converted into vibrational energy and a large fraction of it, at least the energy difference between a 400 nm photon and the L_Q state (*i.e.* about 1 to 1.2 eV), should be located on the initially excited porphyrin unit. Therefore, the TA spectrum directly after internal conversion should correspond to that of the S_1 state with one vibrationally hot porphyrin unit. Vibrational cooling of this unit is responsible for the dispersive feature in the DADS. Indeed, vibrationally hot ground states appear in TA spectra as a positive band on the low energy side of a bleach.[66,67] From these TA measurements, it appears that the small fluorescence quantum yield of the arrays in toluene is due to a fast (~100 ps) $S_1 \rightarrow S_0$ internal conversion. The origin of such a process will be discussed in the next section.

In benzonitrile, $L_Q \rightarrow S_1$ internal conversion can also be observed within the first picosecond after excitation. Once this process is over, the temporal evolution of the TA spectra differs considerably from that in toluene (Fig. 6A and B and Fig. S6, ESI†). For array **1**, the TA spectra exhibit the features assigned above to the S_1 state as well as a positive band at 415 nm that is more pronounced than in toluene. All these bands decay within a few ps and the ensuing spectrum consists of a dispersive-like band centred around 430 nm, similar to that previously ascribed to a vibrationally hot porphyrin unit and decreasing to zero within a few tens of picoseconds. The spectral evolution for **2** is qualitatively similar but somewhat slower (Fig. S6, ESI†).

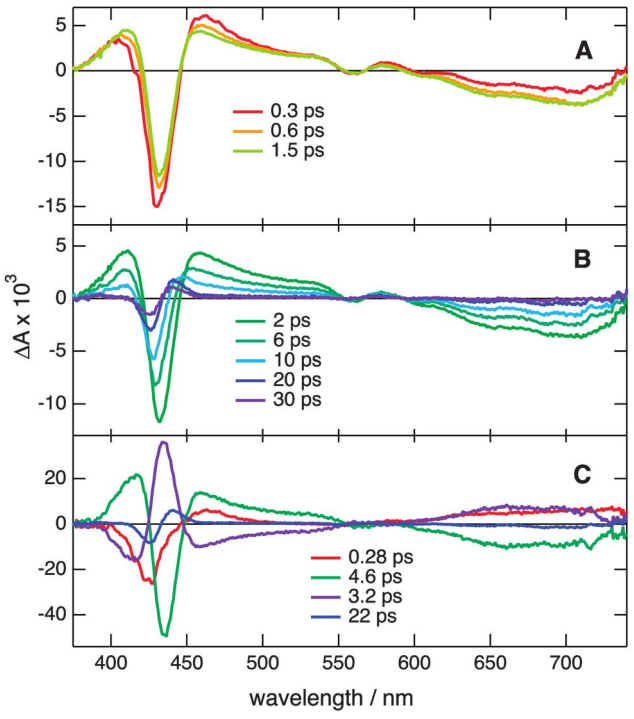

Fig. 6 (A and B) Transient absorption spectra measured at several time delays after $L_B \leftarrow S_0$ excitation of **1** in benzonitrile and (C) decay-associated difference spectra obtained from a global multiexponential analysis.

Global analysis of the temporal evolution of the TA spectra of **1** required the sum of four exponential functions with the time constants listed in Table 2 and the DADS shown in Fig. 6C.

The shortest time constant DADS is similar to that measured in toluene and can be likewise ascribed to $L_Q \rightarrow S_1$ internal conversion. The next two time constants are very similar, 3.2 and 4.6 ps, with the latter equal to the S_1 fluorescence lifetime measured by FU. The 3.2 ps DADS corresponds to an increase of the TA band at 410 and 460 nm as well as an increase of the bleach of the $L_B \leftarrow S_0$ and $S_1 \leftarrow S_0$ bands, whereas the 4.6 ps DADS points to the opposite behaviour, *i.e.* a decay of all four bands.

Finally, the 22 ps DADS is very similar to that assigned to vibrational cooling in toluene and can be interpreted likewise. The strong decrease of the S_1 state lifetime upon going from the quasi-apolar toluene to the highly polar benzonitrile suggests the occurrence of CS in the latter. As the absorption spectra of the radical ions, mostly anions, of c-NDIs reported in the literature exhibit a substantial dependence on the core substituents,[30,53,55,68–70] the absorption spectrum of the ions of the c-NDI centre cannot be predicted. On the other hand, the absorption spectrum of the ZnP radical anion in THF is characterised by an intense band between 410 and 465 nm with a maximum at *ca.* 455 nm and a much weaker one around 710 nm.[71] The absorption spectrum of the ZnP radical cation does not differ much, with an intense band peaking at 410 nm and a weak and broad one above 600 nm.[72] As a consequence, the positive TA band centred at 415 nm can be ascribed to the ZnP radical ion. However, its assignment to the ZnP cation or anion is difficult and, for the moment, this band will simply be ascribed to a CS state. Therefore, the intermediate time constants, *i.e.* 3.2 and 4.6 ps, can be associated with the charge separation (CS) and the ensuing charge recombination (CR) to the vibrationally hot ground state. As the 4.6 ps time constant also coincides with fluorescence decay of the S_1 state, it can be ascribed to the CS, whereas the 3.2 ps time constant to CR. CR in array **1** is thus faster than CS, explaining the small amplitude of the 415 nm band. In such a case, the observed kinetics of the CS population is inverted,[73] *i.e.* the rise time of the CS band corresponds to the CR time constant, whereas its decay time is associated with the CS time constant.

For array **2**, three exponential functions were enough to reproduce the data satisfactorily (Table 2 and Fig. S6, ESI†). The shortest time constant can be assigned to $L_Q \rightarrow S_1$ internal conversion, and the next one, *i.e.* 13 ps, to the decay of the S_1 state as it is close to the 12 ps fluorescence lifetime (Table 1). Its DADS points to an increase of the TA intensity in the 420 nm region and around 710 nm (Fig. S6, ESI†). Here again these features can be assigned to a CS state. Both FbP radical cation and anion exhibit an intense absorption band that overlaps

with the B band of FbP and weaker bands above 600 nm,[74,75] and therefore, the nature of this CS state cannot be deduced from the DADS. Finally, the 33 ps DADS corresponds to the decay of the positive bands ascribed to the CS state and to the ground-state recovery, and can thus be interpreted as the CR time constant. This process is slower than vibrational cooling and, therefore, the vibrationally hot ground state does not contribute significantly to the TA spectra.

$S_1 \leftarrow S_0$ excitation

TA measurements were also performed with 670 nm pump pulses to better disentangle internal conversion and CS dynamics. At this wavelength, excitation of array **1** is entirely due to the $S_1 \leftarrow S_0$ transition. For array **2**, a small interaction with the $L_Q \leftarrow S_0$ cannot be excluded, but it should not be dominant.

At early times, the TA spectra measured with both pentads in toluene (Fig. 7A and Fig. S7, ESI†) show negative features at 420 nm and above 600 nm that can be ascribed to the depletion of the ground state population. The negative band above 600 nm seems to be more structured, with a maximum at *ca.* 710 nm, than with 400 nm pump pulses. The relative intensity of the 420 nm bleach is substantially smaller than in the initial TA spectra upon 400 nm excitation, which is in agreement with a reduced contribution of the porphyrins to the S_1 state. Moreover, the ultrafast initial decrease of the 420 nm bleach and the parallel increase of the bleach above 600 nm found with 400 nm pump pulses are absent. This is an additional confirmation of its assignment to the $L_Q \rightarrow S_1$ internal conversion. As the time delay increases, the overall TA intensity decreases to zero on the ~100–200 ps timescale. During this process, a marked change of the shape of the negative band above 600 nm can be observed and, after about 30 ps, this band has a similar shape as that upon 400 nm excitation. The time evolution of the TA spectra could be analysed globally using the sum of two exponential functions with the time constants listed in Table 2 and the DADS shown in Fig. 7B and Fig. S7, ESI.† Both time constants are the same as the two longest time constants found with 400 nm pump pulses. The larger can be similarly assigned to the decay of the S_1 state population.

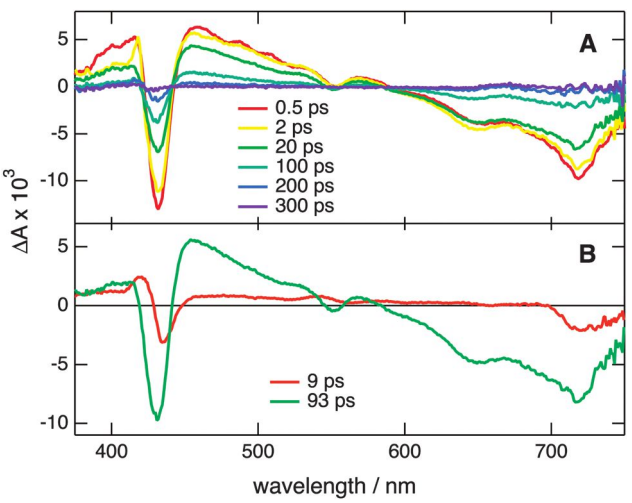

Fig. 7 (A) Transient absorption spectra measured at several time delays after $S_1 \leftarrow S_0$ excitation of **1** in toluene at 670 nm and (B) decay-associated difference spectra obtained from a global multiexponential analysis.

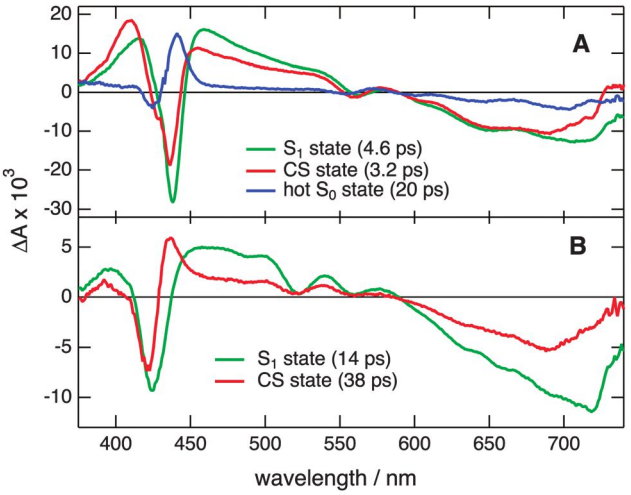

Fig. 8 Species-associated difference spectra obtained from global target analysis of the TA spectra measured with (A) **1** and (B) **2** in benzonitrile upon 670 nm excitation.

The smaller time constant, *i.e.* 9 ps for **1** and 28 ps for **2**, although not much different from that found upon 400 nm excitation seems to be due to a different process than vibrational cooling as the DADS differs considerably. This agrees with the small excess excitation energy at 670 nm. A possible interpretation of this time constant will be proposed in the next section.

In benzonitrile, the TA spectra measured upon $S_1 \leftarrow S_0$ excitation are qualitatively very similar to those recorded after $L_B \leftarrow S_0$ excitation, except for the initial change due to $L_Q \rightarrow S_1$ internal conversion. For **1**, global analysis of the TA data could be performed with three exponential functions with time constants and DADS very similar to those of the three larger time constants found with 400 nm pump pulses (Table 2). Target analysis of the TA data assuming an A → B → C → D scheme was also performed and yielded the same three time constants, as expected,[65] together with the species associated difference absorption spectra (SADS) shown in Fig. 8A. As discussed above, species A corresponds to the S_1 state, B to the CS state, C to the hot ground state and finally D to the relaxed ground state.

A similar result was obtained for **2**, except that two exponential functions were enough to properly reproduce the data (Table 2). As a consequence, target analysis was performed using an A → B → C scheme, with A, B and C corresponding to the S_1 state, CS state and relaxed ground state, respectively. The resulting SADS are shown in Fig. 8B.

$L_Q \leftarrow S_0$ excitation

Finally, similar TA measurements have been repeated upon $L_Q \leftarrow S_0$ excitation, *i.e.* with pump pulses at 550 nm for **1** and 525 nm for **2**. These wavelengths do not coincide with the 0–0 $L_Q \leftarrow S_0$ transition, but ensure a minimum interaction with the broad $S_1 \leftarrow S_0$ band. Overall, the TA spectra of **1** and **2** in toluene and benzonitrile do not differ much from those measured

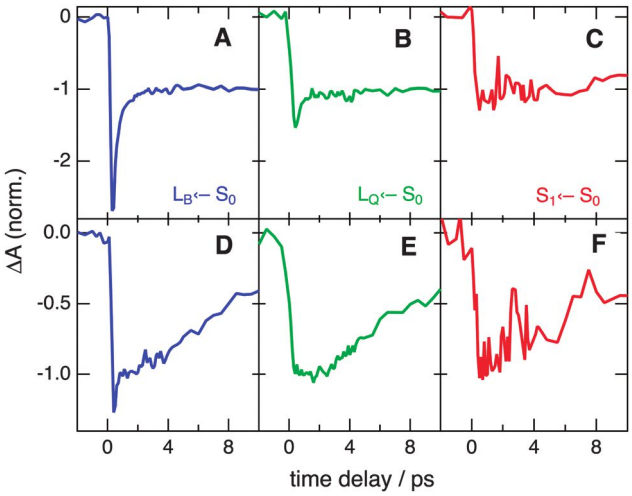

Fig. 9 Transient absorption profiles measured at 428 nm after excitation of **1** in toluene (A–C) and benzonitrile (D–F) at 400 nm (blue), 550 nm (green) and 670 nm (red).

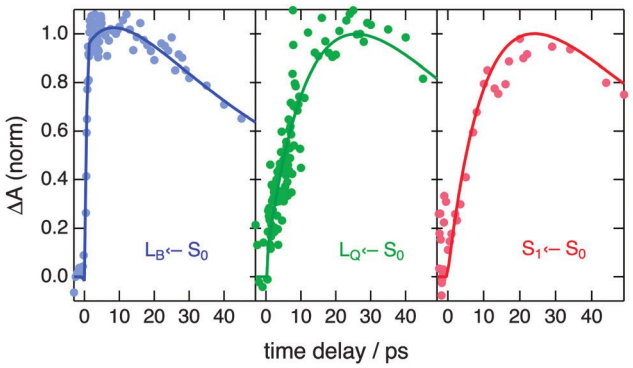

Fig. 10 Transient absorption profiles measured at 436 nm, in the absorption band of the CS state, after excitation of **2** in benzonitrile at 400 nm (blue), 525 nm (green) and 670 nm (red).

upon $L_Q \leftarrow S_0$ and $S_1 \leftarrow S_0$ excitation and only differences in time profiles at selected wavelengths will be discussed here.

The TA profiles at 428 nm, *i.e.* at the maximum of the $L_B \leftarrow S_0$ bleach, measured with **1** in toluene after excitation at the three wavelengths are compared in Fig. 9. The relative amplitude of the fast recovery component, due to $L_Q \rightarrow S_1$ internal conversion, is substantially smaller with 550 nm than with 400 nm pump pulses, whereas it is absent upon 670 nm excitation, as expected. The difference between 400 and 550 nm pump pulses cannot be ascribed to a direct $L_B \rightarrow S_1$ internal conversion as the L_B fluorescence lifetime was found to be smaller than the time constant associated with this fast recovery, but is most probably due to direct excitation of the $S_1 \leftarrow S_0$ transition at 550 nm. Indeed after *ca.* 1 ps, the relative intensities of the 428 nm and >600 nm bleaches are the same as with 670 nm pump pulses, indicating that the whole L_Q population has undergone internal conversion to the S_1 state.

Excitation wavelength dependence can also be observed with **2** in toluene, but the decrease of the relative amplitude of the fast component on going from 400 to 525 nm pump pulses is not as marked as with **1**, *i.e.* only drops from 0.6 to 0.5. The pump wavelength is further from the $S_1 \leftarrow S_0$ band, and thus direct population of the S_1 state is smaller than for **1**.

In benzonitrile, the relative amplitude of the fast recovery component is markedly smaller than in toluene for both pentads (Fig. 9D–F). For **1**, it amounts to *ca.* 0.2 upon 400 nm excitation, whereas it is zero with both 550 and 670 nm pump pulses. With 550 nm pump pulses, a small increase of the bleach during the first 2 ps can even be observed. For **2**, the amplitude of the fast recovery drops from 0.47 to 0.3 on going from 400 to 525 nm excitation, and with 670 nm pump pulses, the bleach increases weakly during the first 5 ps.

This solvent dependence of the bleach recovery dynamics points to the existence of a deactivation pathway of the L_Q state in benzonitrile that competes with internal conversion to the S_1 state and that keeps the ground state of one porphyrin unit depleted. This can also explain why the time constant assigned to $L_Q \rightarrow S_1$ internal conversion is shorter in benzonitrile than in toluene (Tables 1 and 2). The most probable process is CS between a porphyrin unit and the c-NDI centre. This is confirmed by a close inspection of the TA profiles at an absorption wavelength where the CS state absorbs. Fig. 8A shows that the SADS ascribed to the S_1 and CS states of **1** do not differ much and, therefore, the time evolution of the CS state of this array cannot be monitored selectively. This is not the case for **2** whose CS state has a distinct absorption feature at 436 nm (Fig. 8B). The TA profiles measured with **2** in benzonitrile at the three pump wavelengths are illustrated in Fig. 10. They show clearly that the rise of the CS state population is much faster when exciting **2** at 400 nm than at the two longer wavelengths. At 400 nm, the rise is biphasic with a main ~300 fs component and a small ~10 ps component. At 525 and 670 nm, the rise exhibits the slow ~10 ps component only. This slower time constant is similar to the lifetime of the S_1 state and can thus be assigned to the CS from this state. On the other hand, the faster component observed at 400 nm excitation only can be ascribed to the CS from the vibrationally hot L_Q state that competes with internal conversion to the S_1 state.

Most probably, similarly fast CS from the L_Q state is also taking place with **1**. The disappearance of the fast recovery component upon 550 nm excitation on going from toluene to benzonitrile indicates that this CS occurs even if the L_Q state of **1** is not vibrationally hot. In fact, the small increase of the bleach observed during the first 2 ps could arise from this CS. This process should nevertheless be considered as an inherently non-equilibrium or hot CS that cannot be characterised by a rate constant and whose efficiency increases with increasing excess excitation energy.[76]

Discussion

Direction of the CS: hole or electron transfer?

The above results point unambiguously to the occurrence of CS in both pentads in benzonitrile. Porphyrins as well as c-NDIs can in principle act as both electron donors and acceptors,

depending on the nature of the other reaction partner. The direction of the CS, namely from the porphyrin to the excited c-NDI, *i.e.* hole transfer (HT), or *vice versa*, *i.e.* electron transfer (ET), cannot be clearly inferred from the TA spectra. In principle, the energy of the CS states in benzonitrile, E_{CS}, could be estimated from the redox potentials of the donor and acceptor moieties and then compared to the energy of the S_1 state, E_{S1}, to deduce an approximate CS free energy, $\Delta G_{CS} = E_{CS} - E_{S1}$.[77] In the present case, it is however unclear whether the amino groups in the arrays should be associated with the porphyrins or with the c-NDI.

If the energy of the CS product is calculated assuming the latter case and by taking the literature electrochemical data for ZnP ($E_{red} = -1.42$ V, $E_{ox} = 0.82$ V *vs.* SCE),[78] FbP ($E_{red} = -1.21$ V, $E_{ox} = 1.08$ V *vs.* SCE)[78] and an analogue of **3** but with hexyl instead of phenyl substituents ($E_{red} = -1.17$ V, $E_{ox} = 0.52$ V *vs.* SCE),[39] the ET product ($E_{CS,ET}(\mathbf{1}) = 1.95$ eV, $E_{CS,ET}(\mathbf{2}) = 1.74$ eV) is more stable than the HT product ($E_{CS,HT}(\mathbf{1}) = 1.99$ eV, $E_{CS,HT}(\mathbf{2}) = 2.25$ eV).

However, as the energy of the S_1 state, estimated from the absorption and emission spectra, is relatively low, *i.e.* $E_{S1} = 1.7$ eV, this approach indicates that CS from the S_1 state is endergonic in all cases, the less defavourable process being ET from c-NDI to FbP in array **2**, with $\Delta G_{CS} \sim 0.04$ eV. If occurring, it is predicted to be very slow, contrary to the observation.

However, addition of amino groups to tetraphenylporphyrins also substantially increases their electron donating properties.[79] Therefore, the above calculations overestimate the energy of the HT product. The opposite is also true if the reduction potential of the NDI centre and the oxidation potential of aminoporphyrin are taken. A compromise can possibly be obtained by discarding the amino groups and considering CS between NDI and ZnP or FbP. In such a case, HT product states located below the energy of the S_1 state, *i.e.* $E_{CS,HT}(\mathbf{1}) = 1.35$ eV and $E_{CS,HT}(\mathbf{2}) = 1.61$ eV, and thus energetically favourable charge separation are predicted (Table 3).

Hole transfer is also anticipated from the TD-DFT calculations. A CS state associated with a one-electron transition with zero oscillator strength from a MO entirely localised on a porphyrin unit to the LUMO, which is itself on the c-NDI (Fig. 2), is predicted 0.4 and 0.3 eV above the S_1 state for **1** and **2** in toluene, respectively. No CS states associated with a one-electron transition from a NDI to a porphyrin MO could be found up to 0.9 eV above the S_1 state. TD-DFT calculations were also performed with dyads consisting of c-NDI **3** with a single ZnP or FbP substituent. A CS(HT) state located 0.22 and 0.34 eV above the S_1 state was predicted for c-NDI-ZnP and c-NDI-FbP, respectively. Solvation in benzonitrile can be expected to stabilise the CS states by about 0.5 eV, making HT exergonic.

Table 3 Energetic parameters and time constants for charge separation and recombination in benzonitrile

Array	ΔG_{CS}/eV[a]	ΔG_{CR}/eV	τ_{CS}/ps[b]	τ_{CR}/ps[b]
1	−0.35	−1.35	4.6	3.2
2	−0.09	−1.61	13.5	35

[a] Calculated with E_{red}(NDI) = −0.53 *vs.* SCE.[80] [b] Calculated as the average of the time constants determined upon 400 and 670 nm excitation.

CS and CR dynamics in benzonitrile

An energy-level scheme for array **1** based on the above considerations is shown in Fig. 11. For **2**, the scheme is qualitatively similar (Fig. S8, ESI†), except for the L_Q states, which are split into L_{Qx} and L_{Qy} states, with the L_{Qx} state lower by *ca.* 0.2 eV than the L_Q state of **1** and the L_{Qy} state higher by about 0.15 eV. Moreover, the energy of the CS state of **2** should be higher by *ca.* 0.25 eV than that of **1**. This splitting of the L_Q states of FbP has no significant effect on the excited-state dynamics of **2**, as the lifetime of the L_{Qy} state has been shown to be shorter than 100 fs.[81] Therefore, only the L_{Qx} needs to be considered.

The faster CS measured for **1** than for **2** in benzonitrile (Table 3) can be easily explained by a driving force larger by about 0.25 eV. In terms of Marcus theory,[82] CS in the pentads is only weakly exergonic and takes place in the normal regime and, therefore, its rate constant increases with the driving force.

The faster CR measured for **1** than for **2** (Table 3) can also be accounted for by Marcus theory. The CR driving force, $-\Delta G_{CR}$, is equal to the energy of the CS(HT) state and amounts to 1.35 and 1.61 eV for **1** and **2**, respectively. Assuming that the total reorganisation energy is of the order of 1.3–1.5 eV,[83] CR in **1** is essentially barrierless and thus ultrafast, whereas CR in **2** is at the onset of the inverted regime and therefore slower.

It is rather surprising that CS and CR in **1** occur with essentially the same time constants, although CS is much less exergonic than CR (Table 3). This could be explained by a larger electronic coupling for the former, V_{CS}, than for the latter, V_{CR}. This would also account for a CS faster by a factor of 2–3 than CR in **2**. CS involves a hole transfer from the HOMO, that is delocalised over the whole pentad, to a MO localised on a single porphyrin, such as *e.g.* the HOMO-7 shown in Fig. 2. As these two MOs overlap partially, V_{CS} should be substantial. On the other hand, CR involves the recombination of the electron in the LUMO, localised uniquely on the c-NDI, and of the hole on the porphyrin moiety (Fig. 2). In this case, the two singly occupied MOs do not overlap and thus V_{CR} should be small.

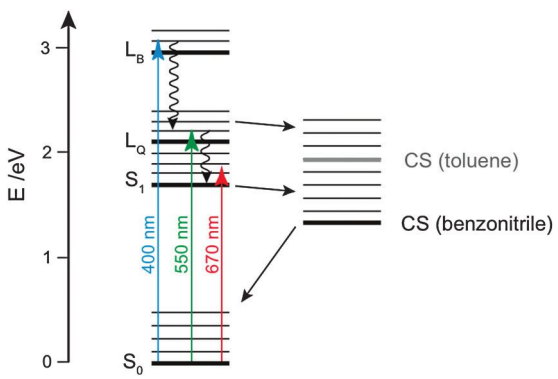

Fig. 11 Energy-level scheme of **1** (the possible splitting of the L_B level due to decreased symmetry and excitonic interaction has been neglected).

Another factor favouring fast CS is the presence of four porphyrins that can all act as electron donors. As a consequence, the probability for CS is four times as large as in a dyad with a single porphyrin. This is not the case for CR that involves only one porphyrin unit.

It should also be noted that both CS and CR in **1** occur on a similar timescale as solvation in benzonitrile, whose average time constant amounts to 5.1 ps.[84] In this case, the similarity of the CS and CR dynamics could also be due to the fact that both the processes are controlled by the dielectric response of the solvent.[85]

The non-equilibrium, hot, CS from the vibrationally unrelaxed L_Q state and the CS from the S_1 state differ considerably. First hot CS is an electron transfer because electronic excitation is localised on a porphyrin unit. Second, the electronic coupling for hot CS should be smaller than that for CS from the S_1 state because it depends on the overlap of a MO localised on a porphyrin unit with the LUMO centred on the c-NDI. Third, only one of the four porphyrin units, *i.e.* the excited one, can act as an electron donor. Despite this, it is much faster and occurs on the sub-picosecond timescale upon excitation to the L_B state. Upon $L_Q \leftarrow S_0$ excitation, it is still operative but slower, of the order of 1 ps, in **1** and no longer takes place in **2**. The free energy for CS from the L_Q state in benzonitrile can be estimated to be *ca.* −0.75 and −0.3 eV for **1** and **2**, respectively. This is more favourable than CS from the S_1 state but should still be in the normal region. Therefore, the process is controlled by a barrier that should be substantially lower in **1** than in **2**. The vibrational temperature reached by the porphyrin moiety upon $L_B \rightarrow L_Q$ internal conversion should greatly help this barrier to be overcome, especially for **2**. This is probably the reason why no hot CS is observed with **2** upon 525 nm excitation. In this case, the excess excitation energy is not sufficient to make CS operative during the lifetime of the L_Q state.

Hot CS takes place on a shorter timescale than the dielectric response of benzonitrile. However, the inertial component of solvation, which is characterised by a 0.3 ps response,[84] probably suffices to bring the CS state at an energy where ET becomes feasible.[86,87]

CS in toluene?

The CS state in toluene can be estimated to be about 0.5 eV less stable than in benzonitrile. For **1**, this state should be located between the S_1 and the L_Q states (Fig. 11), whereas for **2** it should be above the L_Q state (Fig. S8, ESI†). For both pentads however, the CS state should be energetically accessible from the hot L_Q state after internal conversion from L_B. Therefore, hot CS should also be considered in toluene, at least with 400 nm pump pulses. However, as the fluorescence excitation spectra of the pentads are essentially the same as their absorption spectra, this process, if occurring, should be followed by a quantitative recombination to the S_1 state.

Population of the CS state upon 400 nm excitation of **2** in toluene cannot be confirmed from the TA data. At 436 nm, the absorption wavelength of the CS state, a spectral feature ascribed to the vibrationally hot porphyrin was observed. However, a contribution of the CS state to this feature cannot be excluded. Such ultrafast CS and CR to a locally electronic excited state has already been observed with a ZnP containing dyad,[88,89] as well as in the bimolecular quenching of molecules in an upper electronic excited state.[49,90] The net result of this process in the arrays would be the same as the $L_Q \rightarrow S_1$ internal conversion.

S_1 state lifetime in toluene

The S_1 state lifetime of the arrays in toluene is shorter by more than one order of magnitude than that of the model c-NDI **3**. The pentads are relatively flexible, especially around the phenyl group connecting the porphyrin and the c-NDI.[91] As a consequence, at room temperature, they should exist in a relatively wide distribution of conformations with varying conjugation between the porphyrin units and the c-NDI centre that should lead to a fluctuation of the $S_1 \leftarrow S_0$ transition energy. This is confirmed by TD-DFT calculations on the c-NDI-ZnP dyad with different dihedral angles between the porphyrin and the phenyl bridge. The transition energy in the gas phase is predicted to increase from 1.72 eV (721 nm) to 1.8 eV (687 nm) by varying this angle from the optimised value of 67° to 90°. This conformational disorder should lead to some inhomogeneous broadening of the $S_1 \leftarrow S_0$ absorption band. This could explain why the shape of the bleach above 600 nm changes during the first 50 ps after 670 nm excitation. Irradiation in the $S_1 \leftarrow S_0$ absorption band leads to the excitation of a subset of molecules with a similar conformation and thus the initial bleach differs from the absorption band of the ensemble. As conformational fluctuations take place, the shape of the bleach looks more similar to the absorption band of the ensemble. This effect is not observed with 400 nm pump pulses, because in this case, absorption is mostly due to the porphyrin $L_B \leftarrow S_0$ transition, which is not sensitive to the fluctuation of configurations.

We propose that the short excited-state lifetime of the pentads in toluene is due to an efficient internal conversion favoured by (i) a relatively small S_1–S_0 energy gap, (ii) the structural flexibility that modulates the S_1–S_0 energy gap, and (iii) the high density of vibrational states due to the very large size of the chromophore, *i.e.* 382 and 386 atoms for **1** and **2**, respectively.

Excitation energy hopping (EEH)

Whereas the S_1 excitation is spread over the pentads, both L_B and L_Q excitations are in principle localised on a single porphyrin unit. However, the centre-to-centre distance between two adjacent porphyrins, *i.e.* in 2–3 or 6–7 positions, amounts to 11.7 Å in the optimised geometry. Therefore, depending on their strength, Coulombic interactions could result in efficient excitation energy hopping (EEH) in these pairs or even to a delocalisation of the excitation over the pairs. The interaction energy between the $L_B \leftarrow S_0$ transition dipole moments of two adjacent ZnP units, calculated using the point dipole approximation, amounts to *ca.* 250 cm^{-1} (see the ESI† for details), whereas that between the $L_Q \leftarrow S_0$ transition dipole moments is only 20 cm^{-1}. Inserting these values in the Förster equation[92] (see ESI†) yields time constants of 25 fs for L_B EEH and 36 ps for L_Q EEH.

Similarly fast L_B EEH can be expected for **2**. However, because of the splitting of the L_Q states of FbP, L_Q EEH is predicted to be substantially slower in **2**, with a time constant of *ca.* 100 ps (see ESI†). As mentioned above, other conformations of the arrays cannot be excluded. Nevertheless, although the mutual orientation of the porphyrins may differ, the distance between them should be of the same order of magnitude. Considering the distribution of dihedral angles between the porphyrins and the phenyl bridges, the coupling energies should not deviate very much from those estimated here.

Because of the large size of the two quasi-degenerate $L_B \leftarrow S_0$ transition dipole moments, and the small distance between the porphyrins, the point dipole approximation no longer holds and a more precise description of the spatial fluctuation of the charge distributions should be used.[93] Nevertheless, despite the crudeness of the approach, the large coupling energy calculated here points to a substantial excitonic interaction within the porphyrin pairs and to a probable delocalisation of the L_B excitation. This interaction could explain, at least partially, the broadened B band of the pentads.

Given the smaller size of the $L_Q \leftarrow S_0$ transition dipole moments, the coupling energy calculated with the point dipole approximation is more reliable. The substantially smaller coupling energy points to a localisation of the $L_Q \leftarrow S_0$ excitation on a single porphyrin. EEH is in principle possible but is predicted to be considerably slower than internal conversion to the S_1 state or hot CS, and thus should not play a significant role.

Concluding remarks

The two arrays investigated here exhibit a very rich excited-state dynamics that depends on which state is initially populated. Our study reveals that, depending on the excited state considered, these pentads should be viewed as single chromophoric entities, or as genuine multichromophoric arrays. Indeed, the fluorescing excited state is delocalised over the whole array, whereas other upper states are localised on a single porphyrin (*i.e.* the L_Q states) or partially delocalised over pairs of adjacent porphyrins (*i.e.* the L_B states). Therefore, these pentads can be considered as near-IR c-NDI dyes, in fact they are the c-NDIs with the smallest S_1–S_0 gap reported so far, to our knowledge. However, in apolar solvents, where charge separation is not operative, their fluorescence quantum yield is considerably smaller than for most c-NDIs, because of the high efficiency of the internal conversion to the ground state. This process is favoured by the huge size of these molecules, and thus by the very large number of vibrational degrees of freedom that can act as energy accepting modes. In addition to these electronic excited states that can be optically populated, charge-separated states have been shown to play an important role in the photophysics of these arrays. In apolar solvents, although the lowest charge-separated state (with the hole on a porphyrin and the electron on the c-NDI centre) lies above the S_1 state, its presence could accelerate the internal conversion from upper states to the S_1 state *via* non-equilibrium charge separation and recombination.

In polar solvents, this charge-separated state is the lowest singlet excited state and accelerates the non-radiative deactivation of the fluorescent state. It can be populated either from the S_1 state through a thermally activated hole transfer or from the hot L_Q state through a non-equilibrium electron transfer. Because of the small energy gap between this charge-separated state and the ground state, charge recombination is mostly barrierless and thus ultrafast. Therefore, to act as a combined artificial antenna/reaction centre, these pentads should be connected to a secondary electron donor or acceptor, like in natural systems.

Additionally, a consequence of the very large differences in the localisation of the various excitations observed in these arrays is that the electronic coupling for the different charge transfer processes, namely charge separation from the S_1 or L_Q states or charge recombination, differs considerably. This property could be used advantageously, in conjunction with the appropriate energetic parameters, for the design of donor–acceptor systems undergoing ultrafast and long-lived charge separation.

Acknowledgements

This work was supported by the Fonds National Suisse de la Recherche Scientifique through Project No. 200020-147098 and the University of Geneva. S. V. Bhosale gratefully acknowledges the Australian Research Council for support under Future Fellowship through their Discovery program and RMIT University for facilities.

Notes and references

1 V. Sundström, T. Pullerits and R. van Grondelle, *J. Phys. Chem. B*, 1999, **103**, 2327–2346.
2 M. H. Vos and J.-L. Martin, *Biochim. Biophys. Acta*, 1999, **1411**, 1–20.
3 S. Spörlein, W. Zinth, M. Meyer, H. Scheer and J. Wachtweil, *Chem. Phys. Lett.*, 2000, **322**, 454.
4 D. Beljonne, C. Curutchet, G. D. Scholes and R. J. Silbey, *J. Phys. Chem. B*, 2009, **113**, 6583–6599.
5 Y.-C. Cheng and G. R. Fleming, *Annu. Rev. Phys. Chem.*, 2009, **60**, 241–262.
6 R. van Grondelle and V. I. Novoderezhkin, *Nature*, 2010, **463**, 614–615.
7 M. F. Hohmann-Marriott and R. E. Blankenship, *Annu. Rev. Plant Biol.*, 2011, **62**, 515–548.
8 M. Borgström, N. Shaikh, O. Johansson, M. F. Anderlund, S. Styring, B. Aakermark, A. Magnuson and L. Hammarström, *J. Am. Chem. Soc.*, 2005, **127**, 17504–17515.
9 M. R. Wasielewski, *J. Org. Chem.*, 2006, **71**, 5051–5066.
10 I. V. Sazanovich, M. A. H. Alamiry, J. Best, R. D. Bennett, O. V. Bouganov, E. S. Davies, V. P. Grivin, A. J. H. M. Meijer, V. F. Plyusnin, K. L. Ronayne, A. H. Shelton, S. A. Tikhomirov, M. Towrie and J. A. Weinstein, *Inorg. Chem.*, 2008, **47**, 10432–10445.
11 D. Gust, T. A. Moore and A. L. Moore, *Acc. Chem. Res.*, 2009, **42**, 1890–1898.

12 Y. Pellegrin and F. Odobel, *Coord. Chem. Rev.*, 2011, **255**, 2578–2593.
13 F. D'Souza, C. A. Wijesinghe, M. E. El-Khouly, J. Hudson, M. Niemi, H. Lemmetyinen, N. V. Tkachenko, M. E. Zandler and S. Fukuzumi, *Phys. Chem. Chem. Phys.*, 2011, **13**, 18168–18178.
14 B. Grimm, J. Schornbaum, H. Jasch, O. Trukhina, F. Wessendorf, A. Hirsch, T. Torres and D. M. Guldi, *Proc. Natl. Acad. Sci. U. S. A.*, 2012, **109**, 15565–15571.
15 J. Davila, A. Harriman and L. R. Milgrom, *Chem. Phys. Lett.*, 1987, **136**, 427–430.
16 A. Bar-Haim, J. Klafter and R. Kopelman, *J. Am. Chem. Soc.*, 1997, **119**, 6197.
17 F. Li, S. I. Yang, Y. Ciringh, J. Seth, C. H. Martin III, D. L. Singh, D. Kim, R. R. Birge, D. F. Bocian, D. Holten and J. S. Lindsey, *J. Am. Chem. Soc.*, 1998, **120**, 10001–10017.
18 P. Brodard, S. Matzinger, E. Vauthey, O. Mongin, C. Papamicaël and A. Gossauer, *J. Phys. Chem. A*, 1999, **103**, 5858–5870.
19 E. K. L. Yeow, D. J. Haines, K. P. Ghiggino and M. N. Paddon-Row, *J. Phys. Chem. A*, 1999, **103**, 6517–6524.
20 R. F. Kelley, R. H. Goldsmith and M. R. Wasielewski, *J. Am. Chem. Soc.*, 2007, **129**, 6384–6385.
21 N. Aratani, D. Kim and A. Osuka, *Acc. Chem. Res.*, 2009, **42**, 1922–1934.
22 Y. Terazono, G. Kodis, P. A. Liddell, V. Garg, T. A. Moore, A. L. Moore and D. Gust, *J. Phys. Chem. B*, 2009, **113**, 7147–7155.
23 C. Kirmaier, H.-e. Song, E. Yang, J. K. Schwartz, E. Hindin, J. R. Diers, R. S. Loewe, K.-y. Tomizaki, F. Chevalier, L. Ramos, R. R. Birge, J. S. Lindsey, D. F. Bocian and D. Holten, *J. Phys. Chem. B*, 2010, **114**, 14249–14264.
24 E. Maligaspe, T. Kumpulainen, N. K. Subbaiyan, M. E. Zandler, H. Lemmetyinen, N. V. Tkachenko and F. D'Souza, *Phys. Chem. Chem. Phys.*, 2010, **12**, 7434–7444.
25 J. Iehl, J.-F. Nierengarten, A. Harriman, T. Bura and R. Ziessel, *J. Am. Chem. Soc.*, 2011, **134**, 988–998.
26 M. C. O'Sullivan, J. K. Sprafke, D. V. Kondratuk, C. Rinfray, T. D. W. Claridge, A. Saywell, M. O. Blunt, J. N. O'Shea, P. H. Beton, M. Malfois and H. L. Anderson, *Nature*, 2011, **469**, 72–75.
27 F. Zieschang, A. Schmiedel, M. Holzapfel, K. Ansorg, B. Engels and C. Lambert, *J. Phys. Chem. C*, 2013, **117**, 19816–19831.
28 L. L. Miller and K. R. Mann, *Acc. Chem. Res.*, 1996, **29**, 417–423.
29 S. Bhosale, S. A. L. P. Talukdar, A. Fürstenberg, N. Banerji, E. Vauthey, G. Bollot, J. Mareda, C. Röger, F. Würthner, N. Sakai and S. Matile, *Science*, 2006, **313**, 84–86.
30 N. Sakai, A. L. Sisson, T. Bürgi and S. Matile, *J. Am. Chem. Soc.*, 2007, **129**, 15758–15759.
31 F. Doria, M. di Antonio, M. Benotti, D. Verga and M. Freccero, *J. Org. Chem.*, 2009, **74**, 8616–8625.
32 B. A. Jones, A. Facchetti, M. R. Wasielewski and T. J. Marks, *Adv. Funct. Mater.*, 2008, **18**, 1329–1339.
33 N. Sakai, J. Mareda, E. Vauthey and S. Matile, *Chem. Commun.*, 2010, **46**, 4225–4237.
34 N. Sakai, M. Lista, O. Kel, S.-i. Sakurai, D. Emery, J. Mareda, E. Vauthey and S. Matile, *J. Am. Chem. Soc.*, 2011, **133**, 15224–15227.
35 T. C. Barros, S. Brochsztain, V. G. Toscano, P. Berci Filho and M. J. Politi, *J. Photochem. Photobiol., A*, 1997, **111**, 97–104.
36 S. Alp, S. Erten, C. Karapire, B. Koz, A. O. Doroshenko and S. Icli, *J. Photochem. Photobiol., A*, 2000, **135**, 103–110.
37 P. Ganesan, J. Baggerman, H. Zhang, E. J. R. Sudholter and H. Zuilhof, *J. Phys. Chem. A*, 2007, **111**, 6151–6156.
38 F. Würthner, A. Shahadat, C. Thalacker and T. Debaerdemaeker, *Chem.–Eur. J.*, 2002, **8**, 4742.
39 C. Röger and F. Würthner, *J. Org. Chem.*, 2007, **72**, 8070–8075.
40 S. Chopin, F. Chaignon, E. Blart and F. Odobel, *J. Mater. Chem.*, 2007, **17**, 4139–4146.
41 F. Chaignon, M. Falkenstrom, S. Karlsson, E. Blart, F. Odobel and L. Hammarström, *Chem. Commun.*, 2007, 64–66.
42 C. Röger, M. G. Müller, M. Lysetska, Y. Miloslavina, A. R. Holzwarth and F. Würthner, *J. Am. Chem. Soc.*, 2006, **128**, 6542–6543.
43 B. Robotham, K. A. Lastman, S. J. Langford and K. P. Ghiggino, *J. Photochem. Photobiol., A*, 2013, **251**, 167–174.
44 N. Banerji, S. V. Bhosale, I. Petkova, S. J. Langford and E. Vauthey, *Phys. Chem. Chem. Phys.*, 2011, **13**, 1019–1029.
45 D. Villamaina, S. Bhosale, S. J. Langford and E. Vauthey, *Phys. Chem. Chem. Phys.*, 2013, **15**, 1177–1187.
46 K. Rurack and M. Spieles, *Anal. Chem.*, 2011, **83**, 1232–1242.
47 P.-A. Muller, C. Högemann, X. Allonas, P. Jacques and E. Vauthey, *Chem. Phys. Lett.*, 2000, **326**, 321–327.
48 A. Fürstenberg and E. Vauthey, *Photochem. Photobiol. Sci.*, 2005, **4**, 260–267.
49 A. Morandeira, L. Engeli and E. Vauthey, *J. Phys. Chem. A*, 2002, **106**, 4833–4837.
50 G. Duvanel, J. Grilj, H. Chaumeil, P. Jacques and E. Vauthey, *Photochem. Photobiol. Sci.*, 2010, **9**, 908–915.
51 A. Furstenberg and E. Vauthey, *J. Phys. Chem. B*, 2007, **111**, 12610–12620.
52 G. Duvanel, J. Grilj, A. Schuwey, A. Gossauer and E. Vauthey, *Photochem. Photobiol. Sci.*, 2007, **6**, 956–963.
53 N. Banerji, G. Duvanel, A. Perez-Velasco, S. Maity, N. Sakai, S. Matile and E. Vauthey, *J. Phys. Chem. A*, 2009, **113**, 8202–8212.
54 G. Paillotin, C. E. Swenberg, J. Breton and N. E. Geacintov, *Biophys. J.*, 1979, **25**, 513.
55 N. Banerji, A. Fürstenberg, S. Bhosale, A. L. Sisson, N. Sakai, S. Matile and E. Vauthey, *J. Phys. Chem. B*, 2008, **112**, 8912–8922.
56 M. P. Balanay and D. H. Kim, *Phys. Chem. Chem. Phys.*, 2008, **10**, 5121–5127.
57 M. J. Frisch, G. W. Trucks, H. B. Schlegel, G. E. Scuseria, M. A. Robb, J. R. Cheeseman, G. Scalmani, V. Barone, B. Mennucci, G. A. Petersson, H. Nakatsuji, M. Caricato, X. Li, H. P. Hratchian, A. F. Izmaylov, J. Bloino, G. Zheng, J. L. Sonnenberg, M. Hada, M. Ehara, K. Toyota, R. Fukuda,

J. Hasegawa, M. Ishida, T. Nakajima, Y. Honda, O. Kitao, H. Nakai, T. Vreven, J. A. Montgomery Jr., J. E. Peralta, F. Ogliaro, M. Bearpark, J. J. Heyd, E. Brothers, K. N. Kudin, V. N. Staroverov, R. Kobayashi, J. Normand, K. Raghavachari, A. Rendell, J. C. Burant, S. S. Iyengar, J. Tomasi, M. Cossi, N. Rega, J. M. Millam, M. Klene, J. E. Knox, J. B. Cross, V. Bakken, C. Adamo, J. Jaramillo, R. Gomperts, R. E. Stratmann, O. Yazyev, A. J. Austin, R. Cammi, C. Pomelli, J. W. Ochterski, R. L. Martin, K. Morokuma, V. G. Zakrzewski, G. A. Voth, P. Salvador, J. J. Dannenberg, S. Dapprich, A. D. Daniels, Ö. Farkas, J. B. Foresman, J. V. Ortiz, J. Cioslowski and D. J. Fox, Wallingford, CT, 2009.

58 A. Pigliucci, G. Duvanel, L. M. L. Daku and E. Vauthey, *J. Phys. Chem. A*, 2007, **111**, 6135–6145.

59 G. G. Gurzadyan, T.-H. Tran-Thi and T. Gustavsson, *J. Chem. Phys.*, 1998, **108**, 385–388.

60 H. Z. Liu, J. S. Baskin, B. Steiger, C. Z. Wan, F. C. Anson and A. H. Zewail, *Chem. Phys. Lett.*, 1998, **293**, 1–8.

61 H. S. Cho, N. W. Song, Y. H. Kim, S. C. Jeoung, S. Hahn, D. Kim, S. K. Kim, N. Yoshida and A. Osuka, *J. Phys. Chem. A*, 2000, **104**, 3287–3298.

62 A. Morandeira, E. Vauthey, A. Schuwey and A. Gossauer, *J. Phys. Chem. A*, 2004, **108**, 5741–5751.

63 X. Liu, U. Tripathy, S. V. Bhosale, S. J. Langford and R. P. Steer, *J. Phys. Chem. A*, 2008, **112**, 8986–8998.

64 J. Rodriguez, C. Kirmaier and D. Holten, *J. Am. Chem. Soc.*, 1989, **111**, 6500–6506.

65 I. H. M. van Stokkum, D. S. Larsen and R. van Grondelle, *Biochim. Biophys. Acta, Bioenerg.*, 2004, **1657**, 82–104.

66 S. A. Kovalenko, R. Schanz, H. Hennig and N. P. Ernsting, *J. Chem. Phys.*, 2001, **115**, 3256–3274.

67 M. Koch, A. Rosspeintner, K. Adamczyk, B. Lang, J. Dreyer, E. T. J. Nibbering and E. Vauthey, *J. Am. Chem. Soc.*, 2013, **135**, 9843–9848.

68 D. Gosztola, M. P. Niemczik, W. Svec, A. S. Lukas and M. R. Wasielewski, *J. Phys. Chem. A*, 2000, **104**, 6545–6551.

69 I. Pugliesi, P. Krok, S. Lochbrunner, A. Blaszczyk, C. von Hänisch, M. Mayor and E. Riedle, *J. Phys. Chem. A*, 2010, **114**, 12555–12560.

70 R. Bhosale, R. S. K. Kishore, V. Ravikumar, O. Kel, E. Vauthey, N. Sakai and S. Matile, *Chem. Sci.*, 2010, **1**, 357–368.

71 G. L. Closs and L. E. Closs, *J. Am. Chem. Soc.*, 1963, **85**, 818–819.

72 A. N. Okhrimenko, A. V. Gusev and M. A. J. Rodgers, *J. Phys. Chem. A*, 2005, **109**, 7653–7656.

73 C. Högemann and E. Vauthey, *J. Phys. Chem. A*, 1998, **102**, 10051–10059.

74 G. S. Wilson and G. Peychal-Heiling, *Anal. Chem.*, 1971, **43**, 550–556.

75 C. Paliteiro and A. Sobral, *Electrochim. Acta*, 2005, **50**, 2445–2451.

76 A. Rosspeintner, B. Lang and E. Vauthey, *Annu. Rev. Phys. Chem.*, 2013, **64**, 247–271.

77 D. Rehm and A. Weller, *Isr. J. Chem.*, 1970, **8**, 259–271.

78 A. Giraudeau, H. J. Callot and M. Gross, *Inorg. Chem.*, 1979, **18**, 201–206.

79 C.-W. Huang, K. Yuan Chiu and S.-H. Cheng, *Dalton Trans.*, 2005, 2417–2422.

80 S. R. Greenfield, W. A. Svec, D. Gosztola and M. R. Wasielewski, *J. Am. Chem. Soc.*, 1996, **118**, 6767–6777.

81 J. S. Baskin, H.-Z. Yu and A. H. Zewail, *J. Phys. Chem.*, 2002, **106**, 9837–9844.

82 R. A. Marcus and N. Sutin, *Biochim. Biophys. Acta*, 1985, **811**, 265–322.

83 E. Vauthey, *J. Phys. Chem. A*, 2001, **105**, 340–348.

84 M. L. Horng, J. A. Gardecki, A. Papazyan and M. Maroncelli, *J. Phys. Chem.*, 1995, **99**, 17311–17337.

85 I. Rips and J. Jortner, *J. Chem. Phys.*, 1988, **88**, 818.

86 H. Sumi and R. A. Marcus, *J. Chem. Phys.*, 1986, **84**, 4894–4914.

87 N. Banerji, G. Angulo, I. I. Barabanov and E. Vauthey, *J. Phys. Chem. A*, 2008, **112**, 9665–9674.

88 S. Wallin, C. Monnereau, E. Blart, J.-R. Gankou, F. Odobel and L. Hammarström, *J. Phys. Chem. A*, 2010, **114**, 1709–1721.

89 M. V. Rogozina, V. N. Ionkin and A. I. Ivanov, *J. Phys. Chem. A*, 2012, **116**, 1159–1167.

90 P.-A. Muller and E. Vauthey, *J. Phys. Chem. A*, 2001, **105**, 5994.

91 M. P. Eng, T. Ljungdahl, J. Mårtensson and B. Albinsson, *J. Phys. Chem. B*, 2006, **110**, 6483–6491.

92 T. Förster, *Ann. Phys.*, 1948, **2**, 55–75.

93 B. P. Krueger, G. D. Scholes and G. R. Fleming, *J. Phys. Chem. B*, 1998, **102**, 5378–5386.

